Mining tailings as raw materials for reaction-sintered aluminosilicate ceramics: effect of mineralogical composition on microstructure and properties

Marjaana Karhu[1], Juha Lagerbom[1], Soili Solismaa[2], Mari Honkanen[3], Arnold Ismailov[4], Marja-Liisa Räisänen[2], Elina-Huttunen-Saarivirta[1], Erkki Levänen[4] and Päivi Kivikytö-Reponen[1]

[1] VTT Technical Research Centre of Finland Ltd (VTT), P.O.Box 1300, FI-33101 Tampere, Finland

[2] Geological Survey of Finland (GTK), P.O.Box 1237, FI-70211 Kuopio, Finland

[3] Tampere University of Technology, Tampere Microscopy Center, P.O. Box 692, FI-33101 Tampere, Finland

[4] Tampere University of Technology, Laboratory of Materials Science P.O. Box 589, FI-33101 Tampere, Finland

ABSTRACT

This paper presents studies on the utilization of aluminosilicate-based mining tailings as raw materials for mullite-based ceramics. Based on the 3:2 stoichiometric composition, mullite was synthesised by reactive sintering with a series of powder mixtures with alumina additions. X-ray diffractometry and scanning electron microscopy analyses revealed that, at the specific mineralogical composition, mullite structure formed surrounded by an amorphous glass phase in reaction-sintered powder mixtures. Results demonstrated that the chemical and mineralogical composition of mining tailings do have an effect on mullite formation possibilities and, only with the particular mineralogical composition, the mullite formation is possible regardless of the correct Al:Si ratio in tailings. Physical and mechanical properties of the formed ceramics were defined, showing comparable values to 3:2 mullite reference. Mullite structure formation enables a better thermal resistance up to above 1450°C of the formed tailings-based ceramics compared to other aluminosilicates, reflecting their utilization potential for refractory ceramic applications.

Keywords: mining tailings; utilization; mullite; refractory ceramics; reaction sintering

1. INTRODUCTION

Mining tailings are major waste materials from ore processing. In current practice, tailings are transported in a slurry form and stored in impoundments [1]. This causes occupation of large areas of land, costly construction and maintenance activities, potential environmental and ecological risks, e.g. acid mine drainage, and loss of energy and valuable raw materials [2]. In the path towards circular economy, mining tailings are one key resource to be put into reuse and recycling, because of large volumes, environmental impact and need for the efficient exploitation of natural resources [3]. The valorisation of secondary raw materials reduces the risk of poor resource availability while simultaneously decreasing the amount of waste and providing cost-effective reactants for processes [4]. Development of high-value material solutions from secondary raw materials besides high-volume solutions, such as utilization in earth construction, enhances the economic viability of secondary raw materials utilization along with environmental benefits [5].

Mullite, $3Al_2O_3{\cdot}2SiO_2$, is one of the most important aluminosilicate refractory ceramic materials for high-temperature applications such as for refractory bricks, kiln furnitures or protective coatings [6,7,8]. Mullite is the only stable crystalline aluminosilicate phase in the SiO_2–Al_2O_3 binary system, shown detailed in study of Klug et al. (1987) [9]. Mullite has a special combination of properties, such as low density (~3.2g/cm^3), high melting point (~1830 °C) and a low coefficient of thermal expansion (~4.5*10^{-6} K^{-1}) [6]. During the recent years, plenty of research effort has been put on aluminosilicate containing waste utilization in the manufacturing of mullite-based ceramics. In the studies of Alves et al. [5, 10], mullite-based ceramics were prepared by reaction sintering of mixtures containing kaolin clay and kaolin waste. The results showed that the samples derived at 1500°C from formulations containing kaolin waste were composed of acicular mullite and glass phases. In the studies of Dong et al. [11, 12, 13], mullite ceramics were prepared from the mixtures of natural bauxite and industrial waste fly ash. It was suggested that below 1300°C cristobalite reacted with alumina to form secondary mullite. At higher temperatures, bauxite-derived alumina dissolved into a liquid glassy phase, which was formed from the

melted fly ash under the action of different metal oxide impurities. In the study of Jung et al. [14], mullite ceramics were manufactured from appropriate mixtures of coal fly ash and Al_2O_3 powder by reaction sintering at 1500°C. Vieira et al. [15], reported mullite preparation from a mixture of wastes with high contents of silica and aluminium hydroxide: wastes from slate rocks and aluminium sludge from the physicochemical treatment of the wastewaters.

Existing studies suggest the potential of utilizing aluminosilicate-based waste in mullite formation, but further research is needed to fully understand the effects of waste materials composition, particularly the role of impurities, on mullite formation. This paper will provide an insight into the use of aluminosilicate-based mining tailings in mullite synthesis and bridge the most fundamental gaps in the present understanding. Felsic mining tailings (FMT) are side flows rich in quartz and alkali feldspars and, in terms of chemical composition, the dominant oxides are silica (SiO_2) followed by alumina (Al_2O_3) [16]. From the composition point of view, with alumina source addition, the felsic mining tailings hold potential as starting materials for mullite-based ceramics. In the present study, beyond to earlier publications in this field, the utilization of selected felsic mining tailings as raw materials for mullite-based ceramics is examined. The underlying research hypothesis is that, by modifying the raw material chemistry, it is possible to generate mullite-based ceramics from felsic mining tailings. The motivation for the work is that the formation of mullite structure in ceramic materials enables better high-temperature properties compared to other aluminosilicates. The objective in this paper is to investigate and especially to increase the understanding of the effect of chemical and mineralogical composition of felsic-mining tailings on the mullite formation.

2. EXPERIMENTAL PROCEDURE

2.1 Mining tailings

Three Finnish felsic mining tailings were selected for investigation: Molybdenum ore tailings [17], FMT1, Gold ore tailings [18], FMT2, and Quartz ore tailings [19], FMT3. The samples do not represent the whole mining tailings area of their origin, but only the shallow tailings at one sampling point. Surface of the tailing dumpling may differ from the overall composition of the tailing deposit. Table 1 shows the mineralogical analyses of the three mining tailings. Mineralogical characterization included the identification and quantification of mineral phases with scanning electron microscopy (SEM) together with elemental analyses. Table 2 presents the total concentrations of oxides (calculated as oxides) in the tailings, measured with X-ray fluorescence spectrometry (XRF) method. The more detailed explanation of mineralogical analyses, geochemical analyses and sampling procedure are described elsewhere [16]. The mining tailings were selected on the basis of notable differences in quartz and feldspar contents in order to investigate the effects of mineralogy on the mullite formation. Mineralogical analysis of FMT1 showed the quartz content of 40% was about in balance to the sum of feldspars (albite, andesine, K-feldspar). For FMT2, the quartz content was only 11% and the sum of feldspars was much higher, 49%. FMT2 also contained calcite, which was absent or at trace levels in FMT1 and FMT3. The FMT3 differed from FMT1 and FMT2 with its high quartz content, missing alkali feldspars and the presence of kaolinite.

Table 1. Main minerals of the tailing samples (% total area).

Mineral group	Mineral	FMT1	FMT2	FMT3
Quartz	Quartz, SiO_2	40	11	64
Alkali feldspars	Albite, $NaAlSi_3O_8$	23	31	-
	Andesine $(Ca,Na)Al_2Si_2O_8$	12	3	-
	K-feldspar, $KAlSi_3O_8$	6	15	-
K-micas	Biotite, $K(Mg,Fe)_3(Al,Fe)Si_3O_{10}(OH,F)_2$	6	20	-
	Muscovite, $KAl_2(Si_3Al)O_{10}(OH,F)_2$	3	2	27
Clay minerals	Kaolinite, $Al_2(Si_2O_5)(OH)_4$	-	-	4
Carbonate minerals	Calcite, $CaCO_3$	-	6	-

Table 2 shows the total concentrations of phases in the three types of mining tailings. A more detailed explanation of analyses is described elsewhere [16]. In all three mining tailings, SiO_2 was the dominant oxide phase, followed by Al_2O_3, with the overall variation in Si/Al molar ratio being between 3.4 (FMT2) and 14.8 (FMT3). FMT2 contained the greatest share of impurity oxides among the studied mining tailings: CaO, Fe_2O_3, K_2O Na_2O and MgO (~22%), whereas the lowest impurity content was detected for FMT3 (~2%).

Table 2. Chemical composition of the mining tailing samples. Total oxide concentrations measured with XRF method [16].

Sample code	SiO_2	Al_2O_3	Si/Al molar ratio	Fe_2O_3	MgO	CaO	K_2O	Na_2O
FMT1	73.2	11.1	5.6	2.93	4.84	1.95	1.51	3.45
FMT2	57.3	14.3	3.4	5.03	3.14	5.36	4.66	3.91
FMT3	89.8	5.16	14.8	0.57	0.11	0.04	1.2	0.11

2.2 SAMPLE PREPARATION

Aiming at mullite, each mining tailings was mixed with additional alumina source. Recipes shown in Table 3 for reaction sintering experiments were formulated in order to reach the composition of 3:2 mullite ($3Al_2O_3{\cdot}2SiO_2$). The correct Al:Si ratio for mullite composition was balanced by adding commercially available boehmite (aluminum oxide hydroxide, AlO(OH)) powder (provided by Sasol Germany GmbH, average grain size < 0.77 μm) to tailings FMT1, FMT2, FMT3 and the reference sample of kaolinite. Commercial boehmite was used in this study in order to define the behavior differences between the three tailing samples. The portions of boehmite addition were calculated according to chemical composition analysis of mining tailings shown in Table 2. In total, four powder mixtures (one corresponding to stoichiometric mullite composition, three with non-stoichiometric compositions) were formulated for each type of mining tailing by varying the boehmite amount in order to study raw materials composition effects on the formed ceramic structure, Table 3. As a reference, a stoichiometric 3:2 mullite sample was prepared using commercially available kaolinite powder ($Al_2O_32SiO_2{\cdot}2H_2O$ or $Al_2Si_2O_5(OH)_4$)) and aluminium oxide hydroxide (boehmite) powder. Kaolinite was provided by Merck (average grain size < 6.68μm, high kaolin purity).

Table 3. Recipe formulations for reaction-sintered specimens (wt. %).

Recipe code	Stoichiometry	FMT1	FMT2	FMT3	Kaolinite	AlO(OH)
Sint01	stoichiometric	33.6	-	-	-	66.4
Sint02	non-stoichiometric	50.4	-	-	-	49.6
Sint03	non-stoichiometric	67.0	-	-	-	33.0
Sint04	non-stoichiometric	83.5	-	-	-	16.5
Sint05	stoichiometric	-	40.4	-	-	59.6
Sint06	non-stoichiometric	-	55.4	-	-	44.6
Sint07	non-stoichiometric	-	70.5	-	-	29.5
Sint08	non-stoichiometric	-	85.2	-	-	14.8
Sint09	stoichiometric	-	-	28.8	-	71.2

Sint10	non-stoichiometric	-	-	46.4	-	53.6
Sint11	non-stoichiometric	-	-	64.0	-	36.0
Sint12	non-stoichiometric	-	-	82.0	-	18.0
Reference	stoichiometric	-	-	-	51.8	48.2

The mining tailings were received in powder form, but they were first ground by jet milling into the particle size below 10 µm in order to increase the reactivity. The mining tailings were studied as jet-milled and mixed with the alumina source according to Table 3. Powder mixtures were prepared by ball milling in an attrition mill for 30 minutes in air atmosphere. The attrition-milled powders were then uniaxially compressed into green pellets of the size of 20x3 mm using approximately 25 MPa pressure. Heat treatment of green pellets was performed in an ENTECH air chamber furnace in air atmosphere and in ambient air pressure. The heating rate was 3.3 °C/min up to 1300°C with 3 hours holding time at the maximum temperature before cooling to room temperature at the rate of 5 °C/min.

2.3 CHARACTERIZATION METHODS

All three types of mining tailings and all powder mixtures were visually examined after the reaction sintering experiments. In order to understand the differences in behavior between the mining tailing compositions, the thermal behavior of FMT1, FMT2, FMT3 and attrition-milled powder mixtures of stoichiometric mullite composition (Sint01, Sint05, Sint09) was studied using thermogravimetric analysis (TGA, Netzsch STA449 F1 Jupiter) in Differential Scanning Calorimetry (DSC) and thermogravimetry (TG) modes. The tests were conducted in air atmosphere in a temperature range from 40°C to 1300°C at the heating rate of 10 °C/min. In order to verify the differences in melting behavior between the alkali feldspar-containing tailings FMT1 and FMT2, additional heat treatments were carried out in the temperature range of interest, selected based on DSC results.

The thermal expansion and sintering shrinkage behaviors of the stoichiometric mullite powder mixtures (Sint01, Sint05, Sint09) were studied using horizontal pushrod dilatometers (Adamel Lhomargy DI-24 and Netzsch DIL 402 Expedis). The dilatometers require defined specimen dimensions and geometry, limited by the inner dimensions of the heating chambers, geometry of sample holders and maximum travel of the pushrods. Here, the attrition-milled powder mixtures were uniaxially pressed (5 kN) into pellets with a diameter of 11.6 mm. The dilatation was measured in air atmosphere within the temperature range from 20°C to 1450°C and the heating rate of 5 °C/min.

Microstructural analysis of mining tailings and reaction-sintered powder mixtures covered the determination of phase structure and the overall microstructure with compositional analysis of the microstructural details. Phase structure analyses of the materials were performed using X-ray diffractometry (XRD, Empyrean, PANalytical B.V. device, ALMELO) and Cu$K\alpha$ radiation source, and analysed using HighScore Plus software with ICDD database. Microstructural and compositional investigations of the materials were conducted with field emission scanning electron microscopy (FESEM, Zeiss ULTRAplus microscope) and energy-dispersive spectrometry (EDS, INCA Energy 350 with INCAx-act silicon drift detector equipped in FESEM, Oxford Instruments). For microstructural analyses, metallographic cross-sections were prepared by casting cut sections of specimens in Epofix cold setting resin under reduced pressure. The casts were then ground, polished and carbon coated for electrical conductivity. The polished cross-sections were studied by angle-selective backscattered electron (AsB) detector in order to maximize the compositional contrast.

Apparent solid density, bulk density and open porosity of reaction-sintered Sint01, Sint05, Sint09, and the reference samples, all with stoichiometric mullite composition, were investigated according to Archimedes principle following the ISO18754 standard. Compressive strength values were determined for the same materials than the density and porosity values. These were measured using an INSTRON testing system according to the standard ISO 20504:2006. Rectangular samples with dimensions of approximately 15 mm x 40mm were employed in the compression tests, with the used compression speed being 1 mm/min.

3. RESULTS AND DISCUSSION

3.1 THERMAL BEHAVIOR

Compressed pellets of mining tailings (FMT1, FMT2 and FMT3) and all powder mixtures (Sint01-Sint12) were visually examined after the reaction sintering experiments. The observations made after the heat treatments of the specimens are summarized in Table 4. The compressed pellets of pure FMT1 and FMT2 melted completely, losing their shape in the heat-treatment due to melting. On the other hand, no melting was observed for the pellet of FMT3, but the specimen was clearly fractured during the heat treatment. High alkali-feldspar contents of FMT1 and FMT2 tailings compared to that of FMT3 probably caused this difference. As mentioned earlier, feldspars contain alkali metals, which decrease the melting temperature. In the work Raith et al. (2016) [20] feldspars melting behaviour was studied, that supported the observations. All the FMT1 (Sint01-Sint04) and FMT3 (Sint09-Sint12) containing mixtures balanced with boehmite additions retained their shape during reaction sintering. Among the FMT2 containing powder mixtures, only the mixtures (Sint05 and Sint06) with the highest boehmite additions retained their shape during reaction sintering, thus the mixtures Sint07 and Sint08 experienced melting during the heat treatment.

Table 4. Visual observations results after the heat-treatments of the specimens.

Specimen	Composition (wt%)			Observations after heat-treatment at 1300°C/3h
FMT1	Quartz	Alkali feldspars	K-micas	Melted completely, loosing shape
	40	41	9	
FMT2	11	49	22	Melted completely, loosing shape
FMT3	64	-	27	Retained shape, no melting observed but clearly fractured
Sint01	FMT1		Boehmite	Retained shape, no melting observed
	33.6		66.4	
Sint02	50.4		49.6	Retained shape, no melting observed
Sint03	67.0		33.0	Retained shape, no melting observed
Sint04	83.5		16.5	Retained shape, no melting observed
Sint05	FMT2		Boehmite	Retained shape, no melting observed
	40.4		59.6	Retained shape, no melting observed
Sint06	55.4		44.6	Retained shape, no melting observed
Sint07	70.5		29.5	Melting observed
Sint08	85.2		14.8	Melted completely, loosing shape
Sint09	FMT3		Boehmite	Retained shape, no melting observed, but clearly fractured
	28.8		71.2	
Sint10	46.4		53.6	Retained shape, no melting observed
Sint11	64.0		36.0	Retained shape, no melting observed
Sint12	82.0		18.0	Retained shape, no melting observed

Figure 1 shows DSC curves and Figure 2 TG curves for pure mining tailings FMT1, FMT2 and FMT3 and the stoichiometric mullite powder mixtures with boehmite (recipes Sint01, Sint05 and Sint09). For pure tailings, the first phase transformation occurred at 574°C as a small endothermic peak for all three tailing samples. No

notable weight change was related to this phase transformation, based on which the peak could be associated with quartz alfa-beta phase transition, described by Christidis (2010) [21]. With increase in temperature, the DSC curve of FMT2 contained an endothermic peak at approximately 741°C (Fig. 1), connected with weight change by 2.5% in TG curve (Fig. 2). This transformation was probably related to calcite phase decomposition, because FMT2 includes calcite (according to the mineralogy analysis, Table 2). Both FMT1 and FMT2 curves involved also a peak at approximately at 1176°C for FMT1 and at slightly (about 20 ºC) higher temperature for FMT2, relating most probably to the appearance of the liquid phase for both tailings. The DSC curve for FMT3 further included a transformation peak at 820°C (Fig. 1), likely relating to quartz to cristobalite transformation as temperature increases [22].

The curves for powder mixtures with boehmite additions (Sint01, Sint05 and Sint09) all contained the first phase transformation peak at approximately 486°C (Fig. 1) connected with a significant weight change by approximately 10% in TG curve (Fig. 2). This transformation was associated with the boehmite dehydraoxylation (dehydration and simultaneous alumina formation). For powder mixture Sint05, an endothermic peak in a DSC curve appeared at approximately the same temperature than for pure FMT2 tailing and was likely associated with the calcite decomposition process on the basis of the slight further weight loss during the reaction. For the powder mixture Sint_09, the DSC curve included an exothermic peak at slightly above 1200°C, which could indicate the kaolinite transformation to mullite, as earlier reported by MacKenzie et al. (1987) [23].

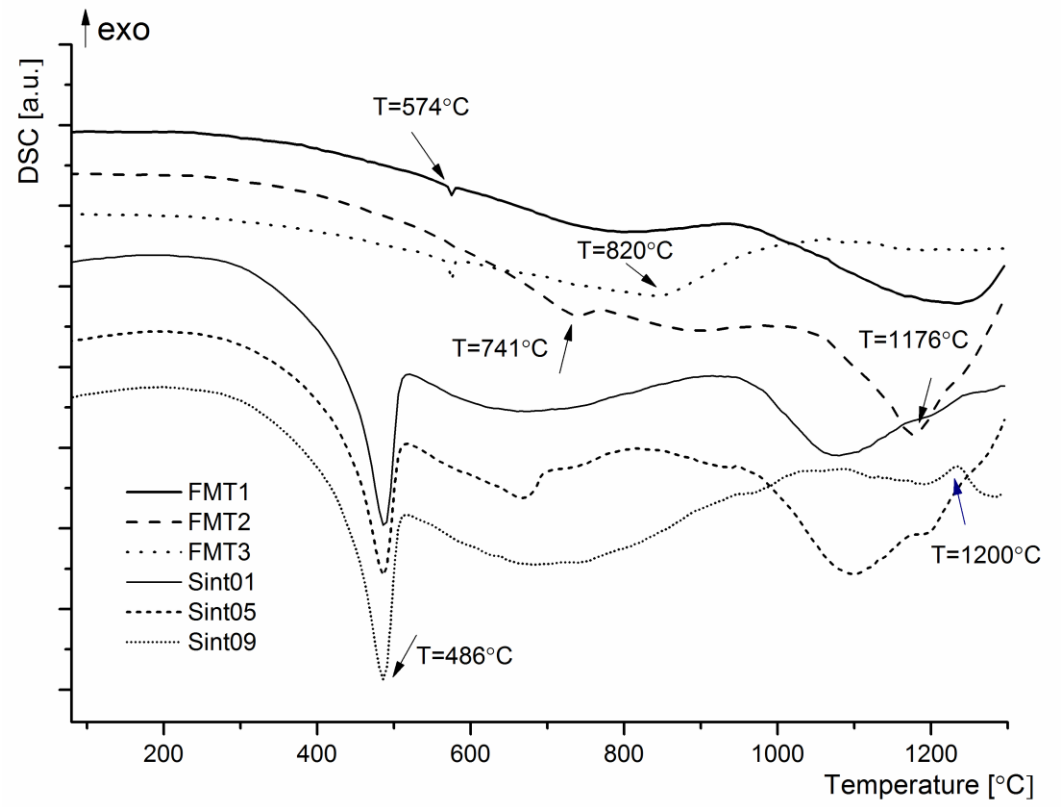

Figure 1. DSC curves for mining tailings FMT1, FMT2, FMT3 and recipes Sint01, Sint05 and Sint09.

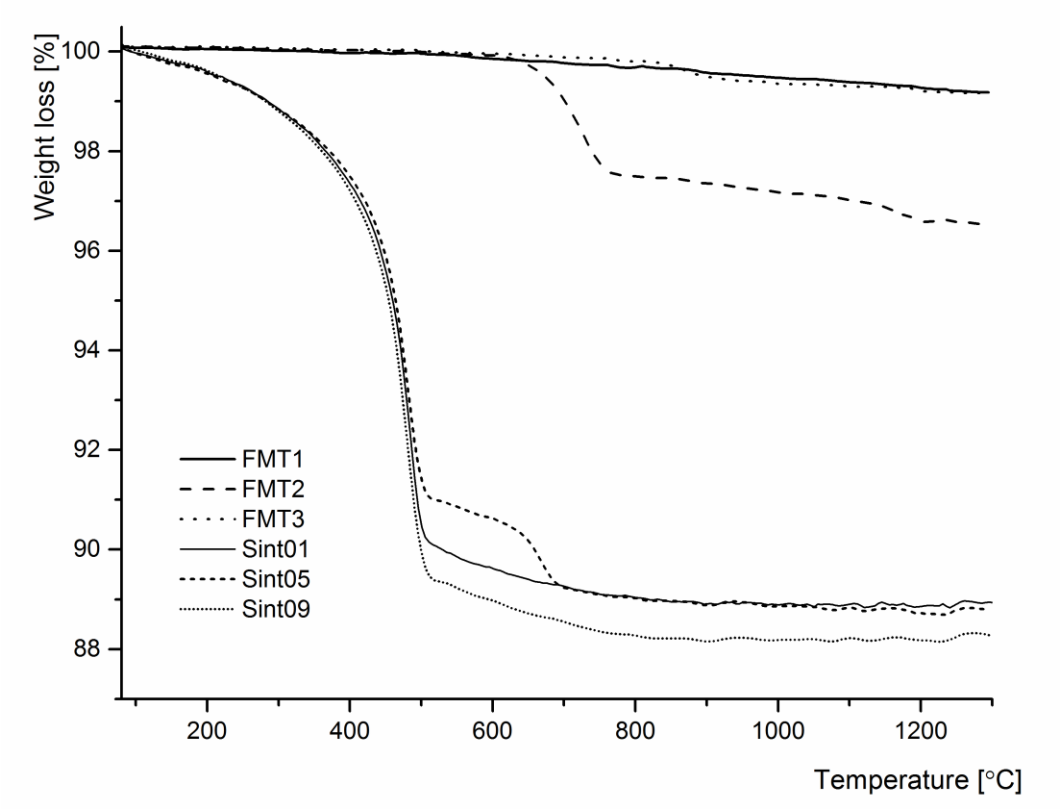

Figure 2. TG curves for mining tailings FMT1, FMT2, FMT3, and selected recipes Sint01, Sint05 and Sint09.

A liquid phase formed most easily in the presence of high-alkali content mining tailings FMT1 and FMT2. DSC curves (Fig. 1) showed for FMT1 and FMT2 a slope decline starting above 900°C and featuring a clear peak approximately at 1176°C for FMT2 and about 30ºC higher temperature for FMT1. FMT3 did not show a similar trend, which could (together with Fig. 1) indicate this transformation was related to the formation of a liquid phase, i.e., melting of FMT1 and FMT2. For FMT2 the decline in the DSC curve slope was steeper as compared to that for FMT1, which could refer to a higher liquid phase amount. Literature shows quite large variation in the melting temperatures of feldspar minerals. For example, for albite, of which FMT1 contains 21% and FMT2 31%, Natrovsky et. al (1982) [24] reported the melting temperatures between 1105-1145˚C, Johnson & McCauleyn (2005) [25] demonstrated the melting temperature of 1134˚C and Sokolář &Vodova (2015) [26] showed melting not until 1180˚C. In order to verify the differences in melting behaviors between FMT1 and FMT2, samples were extra heat treated at the temperature range of interest (1000 ºC -1150ºC). Figure 3 shows compressed FMT1 and FMT2 pellets after heat treatment at three temperatures; 1000°C, 1100°C and 1150°C for 1 hour. Figure shows that in FMT2, the liquid phase formed already between 1000°C and 1100°C, while in FMT1 the liquid phase formation started at somewhat higher temperatures, between 1100 °C and 1150°C.

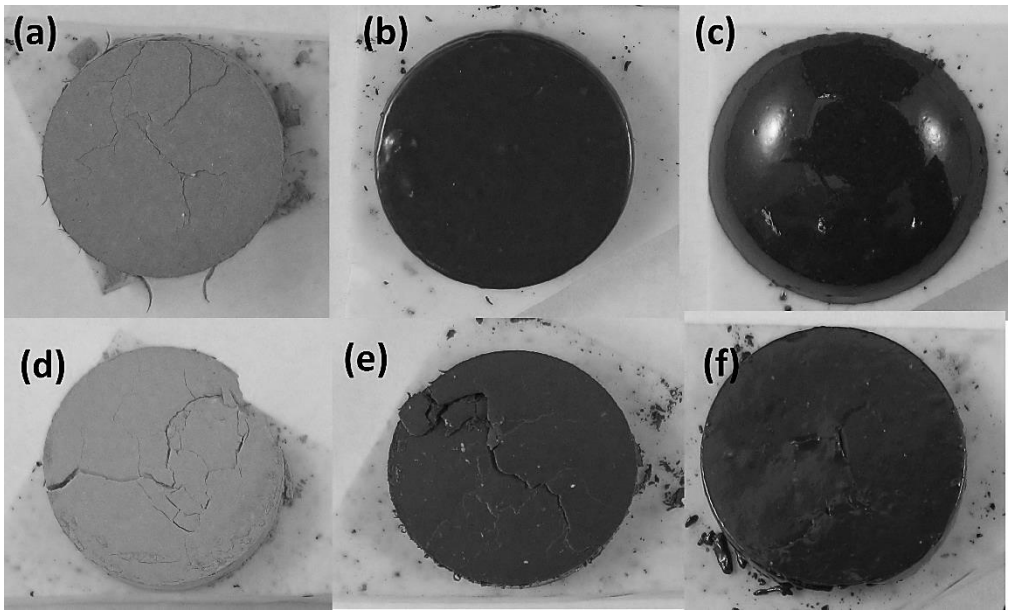

Figure 3. Precompressed tailings FMT1 pellets after heat treatments at (a) 1000°C for 1 hour, (b) 1100°C for 1 hour, (c) 1150°C for 1 hour, and FMT2 after heat-treatments at (d) 1000°C for 1 hour, (e) 1100°C for 1 hour, and (f) 1150°C for 1 hour.

The thermal expansion behavior of the compressed powder mixtures (Sint01, Sint05, Sint09), in the form of dilatometric curves, is presented in Figure 4. The first shrinkage step for all test materials was visible at 500 °C and was attributed to the dehydration of boehmite, as mentioned also in the context of DSC curves. The second, sintering-derived and thus more significant shrinkage of all FMT mixtures (Sint01, Sint05 and Sint09) occurred above 1100°C. Since all of the compressed powder mixtures showed clear evidence of sintering, these results promote the use of the sintering temperature of at least 1300°C for producing dense matter by reaction sintering of raw material mixtures discussed in this paper.

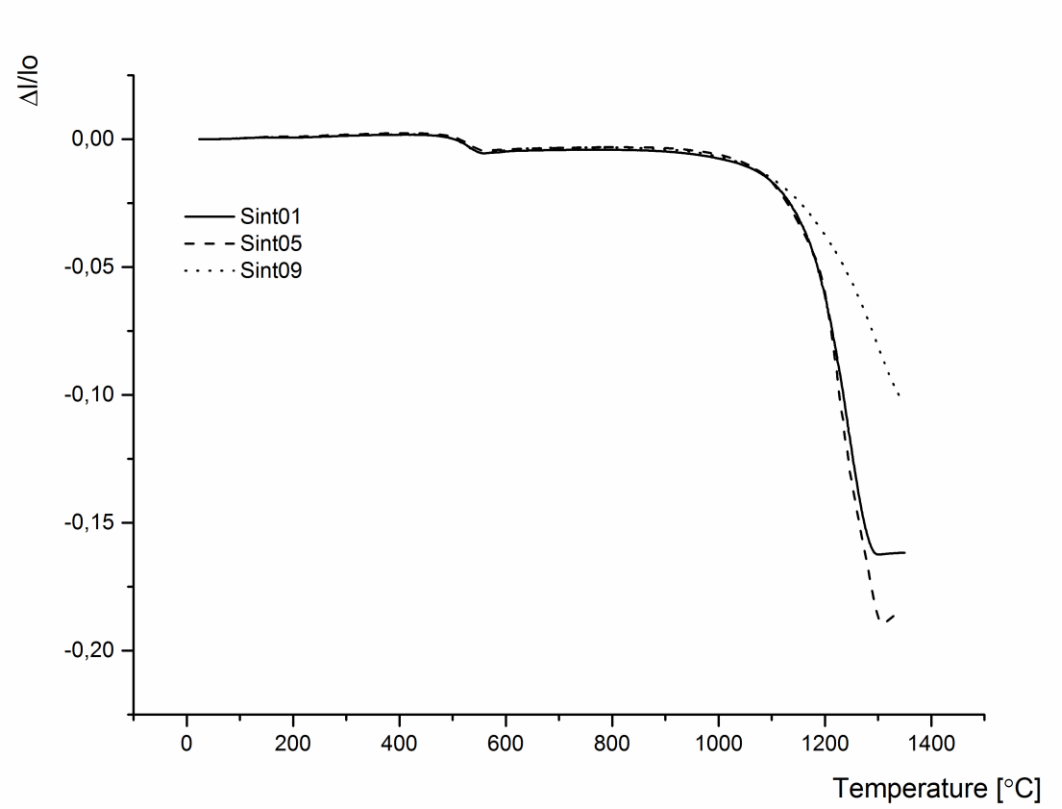

Figure 4. Dilatometric curves of the mixtures Sint01, Sint05 and Sint09.

3.2 PHASE STRUCTURE ANALYSIS

XRD patterns for FMT1, FMT1 after heat treatment, and FMT1 based reaction-sintered powder mixtures (Sint01-Sint04) are shown in Figure 5. The XRD curve for FMT1 powder was characterized by peaks related to quartz, biotite/muscovite and albite phases, consistent with the mineralogy presented in Table 1. FMT1 was completely melted during the heat treatment and, therefore it was crushed in a ball mill before the XRD measurements. The XRD pattern collected for the crushed powder FMT1 after heat treatment showed no peaks of crystalline phases. Hump detected in the curve at low 2θ values may result from the fine structure or even amorphous phase.

All reaction-sintered powder mixtures (FMT1 balanced with boehmite, Table 3) were clearly crystalline and involved mullite as the main crystalline phase. XRD patterns involved also corundum peaks, which indicates some unreacted (dehydrated) boehmite. This finding was further justified by the fact that corundum peak intensities decreased when the boehmite amount in the mixtures decreased. A broad hump between 15° and 30° in XRD patterns indicated the presence of amorphous phase in all reaction-sintered powder mixtures, being most evident in Sint04 curve. According to XRD patterns, the mullite peak intensities decreased and the amorphous phase amounts increased with increase in mining tailings content in the powder mixture recipe. No high-intensity peaks related to the phases identified in the pure tailings: quartz, biotite/muscovite and albite, were seen in XRD spectra for the reaction-sintered mixtures. This is a sign that reaction sintering has been successful.

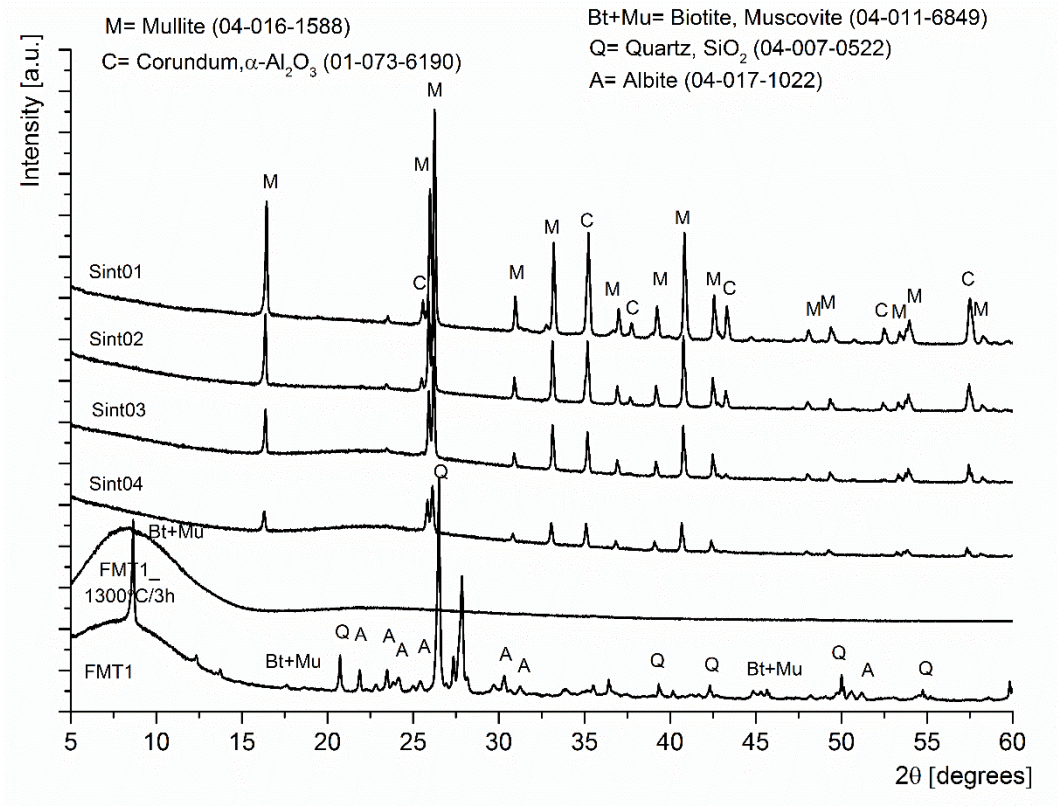

Figure 5. XRD patterns of jet-milled FMT1, heat-treated FMT1 and reaction-sintered pieces Sint01-Sint04.

XRD patterns for FMT2, heat-treated FMT2, and reaction-sintered powder mixture specimens Sint05-Sint08 are shown in Figure 6. In the XRD pattern for FMT2, analysis identified peaks associated with quartz, albite, biotite/muscovite and calcite, in agreement with mineralogical analysis (Table 1). FMT2 was completely melted in the heat treatment, and for that reason, the melted FMT2 sample was crushed in a ball mill into powder form for the XRD measurements. Small corundum peaks detected in the XRD spectrum for melted FMT2 sample were probably due to the contamination from alumina substrate when removing the melted sample.

Conversely to reaction-sintered FMT1 containing mixtures, XRD spectra for FMT2 based powder mixtures (Sint05-Sint08) did not involve mullite peaks after reaction sintering experiments. However, peaks related to at least one crystalline phase could be detected in addition to corundum phase in the XRD patterns for reaction-sintered specimens. Sokolář and Vodova (2015) [26] suggested in their study that sodium-calcium-containing mineral mixture (simulating oligoclase) transformed into the combination of a major phase of anorthite and a minor phase of albite when heated above 1275°C. Also here, anorthite could be suggested as the crystalline phase as a result of andesine transformation or reaction between calcite and albite. A broad hump between 15° and 30° in XRD patterns indicated the presence of an amorphous phase in the reaction-sintered specimens. In addition, for FMT2 containing powder mixtures, no marks from the phases identified in pure FMT2 remained in the sintered mixtures: the peaks related to quartz, albite, biotite/muscovite and calcite had disappeared from the XRD spectra.

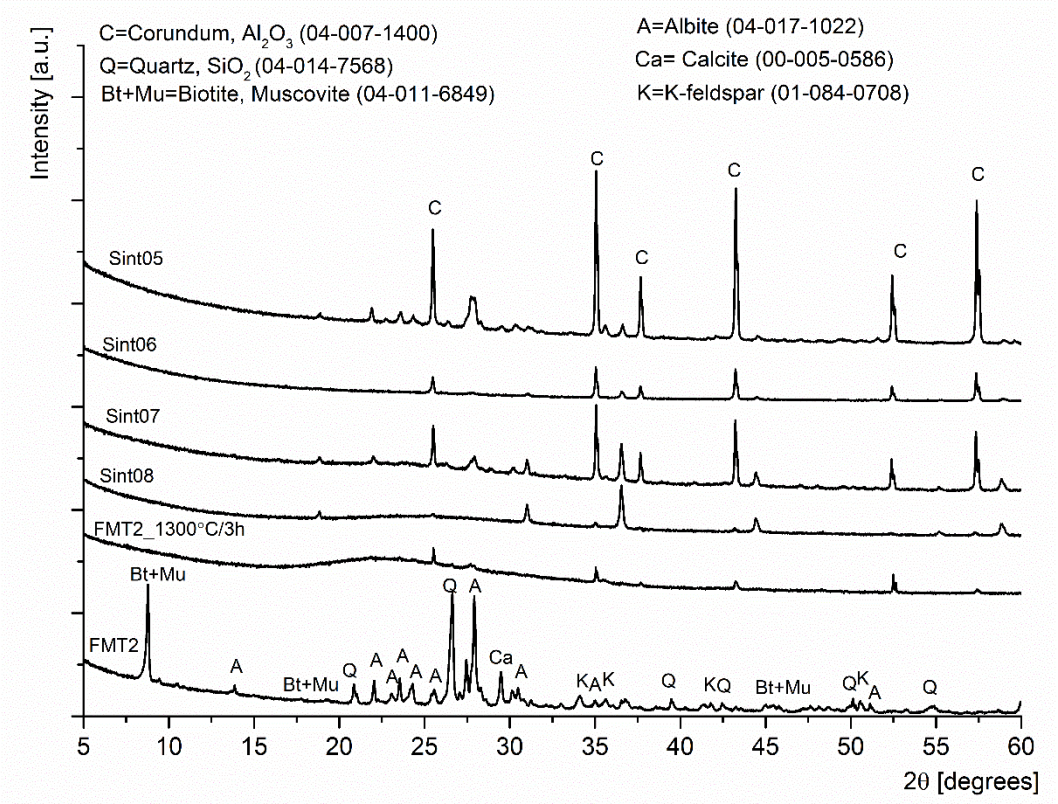

Figure 6. XRD patterns for jet-milled FMT2, heat-treated FMT2 and reaction-sintered pieces Sint05-Sint08.

XRD patterns for FMT3, heat-treated FMT3 and reaction-sintered powder mixtures containing FMT3 (Sint09-Sint12) are shown in Figure 7. The XRD curve for FMT3 contained quartz and muscovite peaks, equally to mineralogical analysis (Table 1). After heat treatment, XRD pattern for FMT3 involved cristobalite peaks and some small peaks related to quartz. Also minor mullite peaks were seen in the XRD curve for the heat-treated mining tailing sample, most probably due to muscovite reaction (all muscovite peaks were disappeared after the heat treatment). Aasly (2008) [22] has shown that the quartz phase transforms into cristobalite at high temperatures, thus evidently this transformation has occurred here. In addition, XRD analyses for reaction-sintered powder mixtures with boehmite additions revealed cristobalite peaks, the intensities of which decreased with increase in boehmite amount. XRD patterns for reaction-sintered powder mixtures also included quartz peaks, indicating that also unreacted quartz was retained in reaction-sintered specimens. The curves also contained peaks associated with mullite and corundum. Corundum peaks were the highest for the mixture of the highest boehmite addition, thus unreacted corundum was retained in the structure. No amorphous hump was detected in the XRD spectra for FMT3 based samples due to the absence of glass formers, like alkali fluxes.

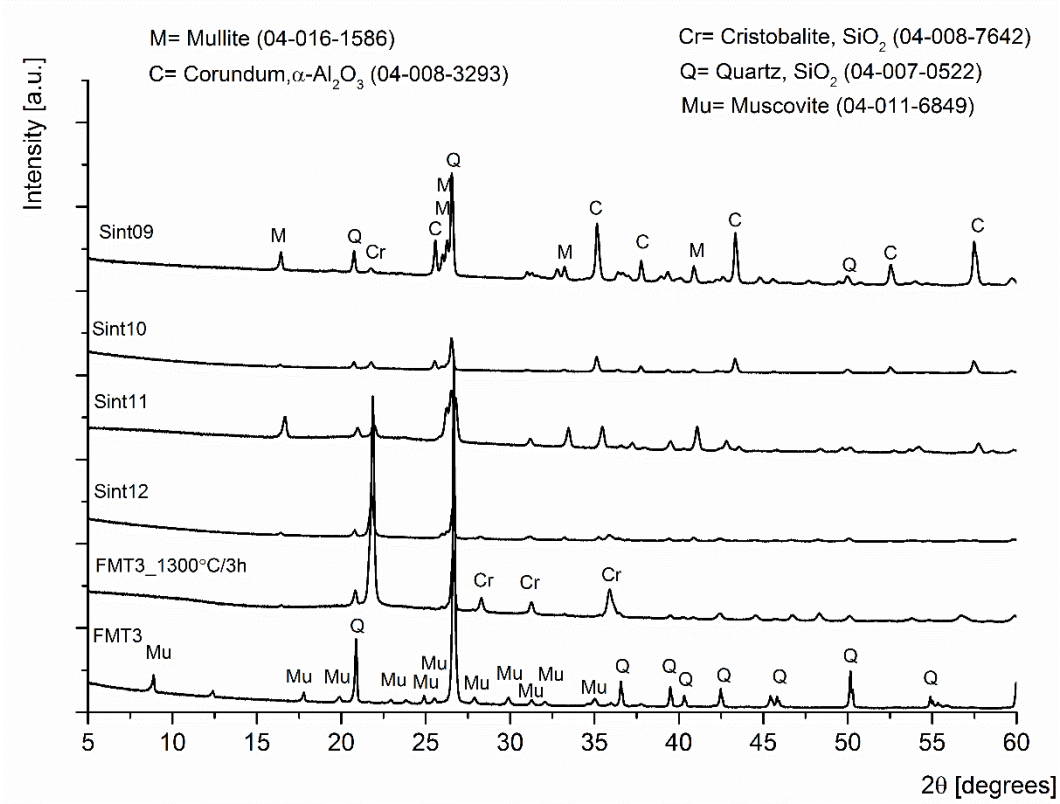

Figure 7. XRD patterns for jet-milled FMT3, heat-treated FMT3 and reaction-sintered pieces Sint09-Sint12.

3.3 MICROSTRUCTURE ANALYSIS

FESEM micrographs of reaction-sintered powder mixture specimens (a) Sint01, (b) Sint02, (c) Sint03 and (d) Sint04 consisting of FMT1 with boehmite additions are shown in Figure 8. FESEM images revealed that the microstructures formed in reaction sintering consisted of evenly distributed and networked needle-shaped crystals surrounded by an amorphous glass phase (seen as uniform areas between the networked needles). Microstructure also involved separate randomly distributed clusters of nearly equiaxed crystals. Porosity, seen in black contrast, was also present in most cases, particularly in Sint01.

EDS analyses together with XRD results enabled to identify the crystalline needle network as the mullite phase (with Al/Si ionic ratio of the 3:1 corresponding to 3:2 mullite). Separate clusters of equiaxed crystals were identified as the corundum phase. Crystalline phases were surrounded by an amorphous aluminosilicate glass phase with traces (~2 wt.%) of Na, K and Ca. According to EDS analyses, it is challenging to draw any definite conclusion about the Fe distribution, due to complexity of microstructural details and fine crystal size compared to electron beam size and analysis spot dimension exceeding the crystal detail size. According to EDS analyses, Fe was present in the amorphous phase but traces of it were detected also in the mullite needles. FMT1 contained 6% biotite, which is a Fe-rich mineral, which could partly explain the presence of Fe in the mullite needles. Microstructural images support the observations based on the XRD curves that the amount of amorphous phase increased with decrease in the amount of boehmite.

XRD, SEM and EDS analyses suggested that, during the reaction sintering of FMT1 containing mixtures, Sint01, Sint02, Sint03 and Sint04, the original minerals included in FMT1, i.e., alkali feldspars and K-micas, converted into liquid form. Higher temperature increased the solubility of silica to the melt, which enabled silica reaction with alumina (resulting from boehmite). Mullite phase then crystallized from the aluminosilicate melt. According to Schneider et al. (2008) [6], mullite crystals that have grown from aluminosilicate melt usually display acicular (needle-shaped) morphology, which also supports this assumption.

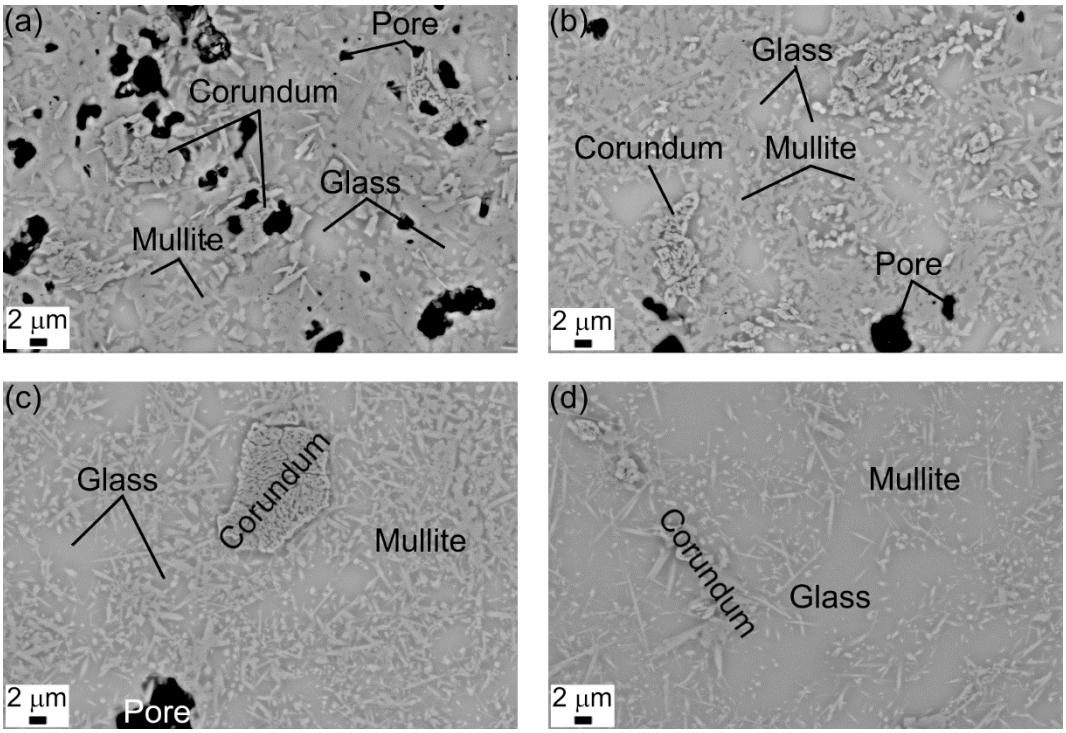

Figure 8. FESEM images (AsB) of the cross-sections of at 1300°C for 3 hours reaction-sintered (a) Sint01, (b) Sint02, (c) Sint03, and (d) Sint04 specimens.

Figure 9 shows FESEM micrographs of reaction-sintered powder mixture specimens of (a) Sint05 consisting of FMT2 and (b) Sint09 consisting of FMT3 with boehmite additions. The microstructure formed from FMT2 containing powder mixture (Fig. 9 a) contained needle-shaped crystals with the length of approximately 5-10 μm and surrounded by an amorphous phase. In addition, here, randomly distributed crystal clusters appeared in occasional areas; these were identified as corundum according to combined EDS and XRD analyses. According to EDS analyses, the crystal needles were identified as an Al-rich aluminosilicate phase. One possibility is that calcite is reacting in feldspar melt and crystallized into anorthite as suggested in XRD results.

As a conclusion, it seems that also in the case of FMT2, the original phases of albite, biotite, K-feldspar and quartz did melt and formed a new aluminosilicate crystalline phase. For some reason, mullite was not detected after the reaction sintering process regardless of the correct Al:Si ratio in the Sint05 mixture. Sint05 contains FMT2, in which the amount of impurities was the highest among the studied mining tailings (FMT1, FMT2, FMT3).

FESEM examinations, Figure 9 (b), revealed that Sint09 specimen that contains FMT3 with boehmite addition had a microstructure consisting mainly of coarse grains. There were also visible macro cracks in the structure. According to EDS analyses, the coarse grains were identified as quartz grains, which is supported by XRD analyses. Corundum crystals were identified between the quartz grains and, to some extent, their clustering was observed. Occasional single mullite needles were identified according to EDS analyses, probably resulting from kaolinite heating. These results suggest for FMT3 with low alkali content and high silica content that much of the quartz phase was retained unreacted in the reaction sintering experiments. It could be possible to facilitate mullite formation with notably higher sintering temperatures. For example, the mullitization temperature for the solid-state reaction between Al_2O_3 and SiO_2 particles can be higher than 1650°C for the completion of the reaction.

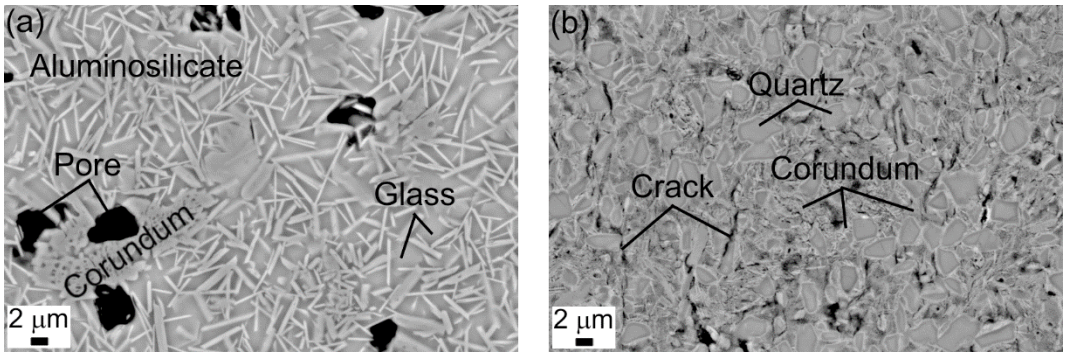

Figure 9. FESEM images (AsB) of cross-sections of at 1300°C for 3 hours reaction-sintered (a) Sint05, and (b) Sint09 specimens.

Presented results showed that mullite crystallizes from aluminosilicate melt in alkali-feldspar- and quartz-containing tailing, FMT1, mixed with boehmite. However, mullite does not form in the mixtures of FMT2 bearing higher alkali-feldspar and lower quartz content as compared to FMT1. According to the received results, it is suggested that only with a particular mineralogical composition the mullite formation is possible regardless of the correct Al:Si ratio. It seems that one important factor in mining tailing mineralogical composition for the following mullite formation is the amount of alkali feldspars in relation to quartz. Mineralogical analysis for FMT1 (Tables 1 and 2) shows that the quartz content was about equal to the sum of alkali feldspars. For FMT2, the quartz content was only 11% and the alkali feldspars content was relatively much higher. Another mineralogical difference between the studied mining tailings FMT1 and FMT2 was the Fe-containing micas. In FMT2, the amount of mica was relatively much higher (20% compared to 6% in FMT1).

In the study by Sokolář and Vodova (2015) [26] it was shown that the melting of feldspars is dependent on many factors, such as the rate of heating and the content of alkali oxides. For the melting of feldspars, not just the total content of feldspar components are important, but also the ratio between potassium and sodium feldspars (i.e. between K_2O and Na_2O). At the appropriate ratio, low-melting eutectics may appear, with a melting temperature substantially lower than the melting temperature of pure feldspars. Results presented here suggest that one explanation for the differences for mullite crystallization between the three felsic tailings with different mineralogical compositions could relate to differences in the melting temperatures of FMT1 and FMT2. Results indicate that mullite crystallization in aluminosilicate melt is possible if the crystallization temperature for mullite is high enough. For this approach, the composition plays an important role, i.e., the amount of alkalis.

3.4 STRUCTURAL INTEGRITY AND STRENGHT

Table 5 summarizes apparent density, bulk density and open porosity values for the reaction-sintered powder mixture specimens Sint01, Sint05, Sint09 and the stoichiometric 3:2 mullite used as a reference. Results are average values determined for three parallel samples. The results showed that open porosity was much lower for the specimen Sint01 containing FMT1 and Sint05 containing FMT2 that are rich in alkali feldspars compared to Sint09 containing FMT3 that does not contain alkalis. The formed liquid phase clearly promoted the densification of the structure. No clear trends were detected between density values and the specimen composition.

Table 5. Apparent density, bulk density and open porosity values of the studied specimens and reference.

Recipe code	Apparent solid density (g/cm^3)	Bulk density (g/cm^3)	Open porosity (%)
Sint01_1300C/3h	2.7±0.02	2.6±0.05	6.1±1.12
Sint05_1300C/3h	3.0±0.004	2.9±0.005	2.4±0.06
Sint09_1300C/3h	3.1±0.007	2.4±0.02	24±0.71
Reference	3.1±0.001	2.3±0.02	25±0.51

Figure 10 shows the compressive strength values for the reaction-sintered specimens containing FMT1 (Sint01), FMT2 (Sint05), FMT3 (Sint09) and for the reference. Results are average values of five measurements. The results disclosed that the strength values (>60 MPa) of the mining tailing containing specimens were of the same magnitude than for the reference. As porosity results, Table 5, revealed, the formed liquid phase (Sint01 and Sint05) promoted the densification of the specimens, which had a slight positive effect on strength values. Thus, the highest overall strength values were obtained for sample Sint05, with the powder mixtures with the lowest open porosity. Conversely, the lowest strength values were detected for Sint09, being characterised by the highest open porosity. However, the strength values of Sint09 and the reference were still at sufficient level despite of the high porosity in these specimens. The most significant difference between the mining tailing based samples and the reference was the extent of scatter in the strength values: in the case of all mining tailings based samples (Sint01, Sint05, Sint09), the scatter was approximately 2-3 times that in the case of the reference sample. Magnitude of the scatter in strength values was higher than the scatter reported in the works of Alves et al. [5] and Dong et al. [12]. They both reported flexural strength values. This was probably because of a great structural heterogeneity between local areas in the reaction-sintered mining tailing samples, particularly concerning the distribution of the amorphous glass phase.

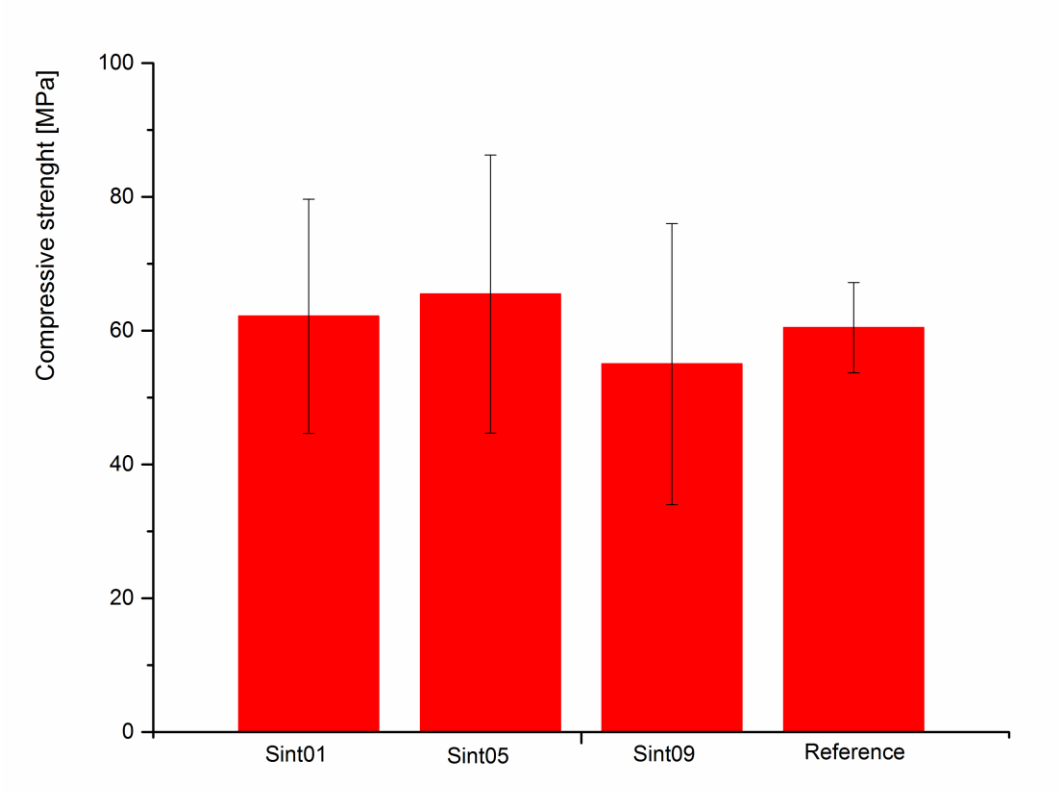

Figure 10. Compressive strength values at 1300°C for 3 hours reaction-sintered specimens.

3.5 MULLITE FORMATION AND THERMAL RESISTANCE

Characterization results showed that high alkali-feldspar content caused pure FMT1 to melt already above 1100°C (Fig. 3). By modifying the chemical composition of the mining tailing with boehmite addition it was possible to generate microstructure that included acicular mullite network surrounded by amorphous glass phase. According to the research hypothesis, the formation of mullite would improve the thermal resistance and enable use at higher temperatures of the formed ceramic materials.

In order to prove the improved thermal resistance of the samples containing mullite structure, the reaction-sintered Sint01, Sint05 and Sint09 pellets from the first dilatometer measurements were subjected again to dilatometer measurements, which were conducted at 1450°C. The results, Figure 11, show a clear difference between Sint01, which contains the mullite structure, and Sint05, where mullite structure was not formed. During reheating Sint05, a clear transformation still occurred, first after 1100°C and second after 1300°C, most probably due to liquid phase formation. In contrast, reheating Sint01 and Sint09 introduced homogenous and linear expansion of the specimen. Small shrinkage occurred after 1300°C, what indicated that the sintering observed in the previous measurements had not been complete. In the forthcoming works, the optimal reaction sintering time and temperature will be studied in more detail. In addition, the high temperature properties of the mullite containing specimens will be studied more thoroughly in order to establish their applicability for refractory uses.

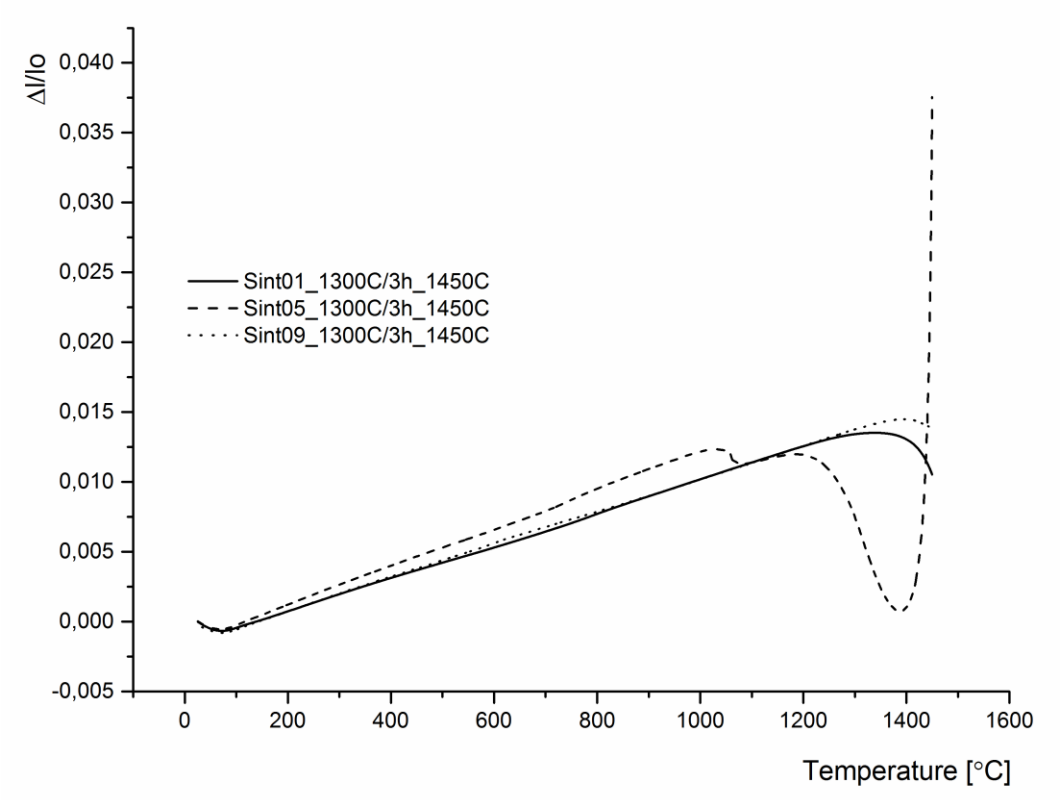

Figure 11. Dilatometric curves of reheating of the reaction-sintered Sint01, Sint05, and Sint09 pellets.

4. CONCLUSIONS

The results of the presented study enable the following conclusions:

1. High alkali-feldspar contents cause molybdenum ore tailings (FMT1) and gold ore tailings (FMT2) to melt already slightly above 1100°C. Therefore, these tailings as such are not suitable for refractory applications requiring thermal resistance up to higher temperatures.

2. XRD, FESEM and EDS analyses suggest that, by reaction sintering at 1300°C for 3 hours with boehmite, molybdenum ore tailings (FMT1) containing powder mixtures yield acicular mullite structure surrounded by amorphous glass phase. During the heat treatment, the original minerals in the tailings: alkali feldspars and K-micas, convert into a liquid form. Higher temperature increases the solubility of silica to the melt, which subsequently enable silica reaction with alumina (resulting from boehmite) into mullite. Thus, mullite phase crystallizes from the aluminosilicate melt.
3. Mullite does not form in the mixtures of gold ore tailings (FMT2), having the highest amount of alkali-feldspars among the three mining tailings, although the aluminosilicate melt forms, similarly to molybdenum ore mining tailing case. According to the results, it is suggested that only with the particular mineralogical composition the mullite formation is possible regardless of the correct Al:Si ratio. One important factor in tailing mineralogical composition with respect to mullite formation is the amount of alkali feldspars in relation to quartz. Excess amount of iron-rich mica minerals may also prevent the mullite formation.
4. In quartz ore tailings (FMT3), aluminosilicate melt does not form and mullite is thus not crystallized from the melt. Reaction-sintered specimens were clearly fractured. For FMT3 with low alkali content and high silica content, the quartz retained largely unreacted in the reaction sintering experiments. It may be possible to facilitate the mullite formation with notably higher sintering temperatures via solid-state reaction between Al_2O_3 and SiO_2 particles.
5. Porosity is much lower in reaction-sintered specimens containing molybdenum ore tailings (<6%) and gold ore tailings as compared to the quartz ore tailings (24%). The liquid phase that form in the two former systems in the presence of boehmite promote the densification of the structure. Molybdenum ore tailings and gold ore tailings containing specimens show compressive strength values (>60 MPa) comparable to the corresponding values for the reference, yet with a greater scatter.
6. Mullite network formation enables better thermal resistance up to >1450°C for the formed ceramic materials as compared to other aluminosilicate phases in the samples, showing potential to be used for refractory ceramic applications.

ACKNOWLEDGEMENT

The research has been supported by the Academy of Finland, project CeraTail funding decision # 292563 and by the Strategic Research Council at the Academy of Finland, project CloseLoop, funding decision #303453.

REFERENCES

[1] Kauppila, P. M., Räisänen, M. L. & Myllyoja, S. 2011. Best Environmental Practices in Metal Ore Mining. Finnish Environment en29/2 011. http://hdl.handle.net/10138/40006 ISSN 978-952-11-3942-0 (PDF)

[2] Akcil, A., Koldas, S. Review article Acid Mine Drainage (AMD): causes, treatment and case studies. Journal of Cleaner Production 14 (2006) 1139-145. https://doi.org/10.1016/j.jclepro.2004.09.006

[3] Lottermoser, B. G. Recycling, Reuse and Rehabilitation of Mine Wastes. *ELEMENTS*, VOL. 7, PP. 405–410. DOI: 10.2113/gselements.7.6.405

[4] EllenMacArthurFoundation. Report Growth within: a circular economy vision for a competitive Europe. *June 2015. Available:* https://www.ellenmacarthurfoundation.org/assets/downloads/publications/EllenMacArthurFoundation_Growth-Within_July15.pdf

[5] Alves, H.P.A., Silva, J.B., Campos, L.F.A., Torres, S.M., Dutra, R.P.S. and Macedo, D. A. Preparation of mullite based ceramics from clay–kaolin waste mixtures, Ceramics International 42 (2016) 19086–19090, https://doi.org/10.1016/j.ceramint.2016.09.068

501 [6] Schneider, H., Schreuer, J., Hildmann, B. Structure and properties of mullite—A review, Journal of the
502 European Ceramic Society 28 (2008) 329–344, https://doi.org/10.1016/j.jeurceramsoc.2007.03.017

503 [7] Paksaresht, A.H. (ed.), Production, Properties, and Applications of High Temperature Coatings. IGI
504 Global 2018, ISSN: 2327-5448

505 [8] Krishnamurthy, R. and Sheldon, B. W. Stability of Mullite Protective Coatings for Silicon-Based Ceramics.
506 J. Am. Ceram. Soc., 88 [5] 1099–1107 (2005). https://doi.org/10.1111/j.1551-2916.2005.00169.x
507

508 [9] Klug, F.J. S. Prochazka, and R.H. Doremus, Alumina–silica phase diagram in the mullite region,
509 *J. Am. Ceram. Soc*. **70**, 750–759 (1987). https://doi.org/10.1111/j.1151-2916.1987.tb04875.x
510

511 [10] Alves, H. P.A., Junior, R.A., Campos, L.F.A., Dutra, R.P.S, Grilo, J.P.F., Loureiro, F.J.A. and
512 Macedo, D.A. Structural study of mullite based ceramics derived from a mica-rich kaolin waste, Ceramics
513 International 43 (2017) 3919–3922, https://doi.org/10.1016/j.ceramint.2016.12.035

514 [11] Dong, Y., Feng, X., Feng, X., Ding, Y., Liu, X and Meng, G. Preparation of low-cost mullite ceramics
515 from natural bauxite and industrial waste fly ash, J. Alloys Compd. 460 (2008) 599–606,
516 https://doi.org/10.1016/j.jallcom.2007.06.023

517 [12] Dong, Y., Zhou, J., Lin, B., Wang, Y., Wang, S., Miao, L., Lang, Y., Liu, X. and Meng, G. Reaction-
518 sintered porous mineral-based mullite ceramic membrane supports made from recycled materials, Journal of
519 Hazardous Materials 172 (2009) 180–186, https://doi.org/10.1016/j.jhazmat.2009.06.148

520 [13] Dong, Y., Hampshire, S., Zhou, J., Lin, B., Ji, Z., Zhang, X., Meng, G. Recycling of fly ash for preparing
521 porous mullite membrane supports with titania addition, Journal of Hazardous Materials 180 (2010) 173–180,
522 10.1016/j.jhazmat.2010.04.010
523

524 [14] Jung, J. S. and Park, H. C. Mullite ceramics derived from coal fly ash, Journal of Materials Science
525 Letters 20 (2001) 1089 – 1091.

526 [15] Vieira, S.C., Ramos, A.S., Vieira, M.T. Mullitization kinetics from silica- and alumina-rich wastes.
527 Ceramics International 33 (2007) 59–66, https://doi.org/10.1016/j.ceramint.2005.07.015
528

529 [16] Solismaa, S., Ismailov, A., Karhu, M., Sreenivasan, H.,Lehtonen, M., Kinnunen, P., Illikainen, M.,
530 Räisänen, M-L. Valorization of Finnish mining tailings for the use of ceramic industry, Bulletin of the
531 Geological Society of Finland 90 (2018) 33–54, https://doi.org/10.17741/bgsf/90.1.002
532

533 [17] Haapala, I., & Rämö, O. Mineral deposits related to granitic rocks. In: W. D. Maier, R. Lahtinen, & H.
534 O'Brien (Eds.) Mineral Deposits of Finland (2015) 531-556. Amsterdam: Elsevier Scientific Publ. Co. DOI:
535 10.1016/B978-0-12-410438-9.00021-2

536 [18] Sorjonen-Ward, P. Hartikainen, A., Nurmi, P. Rasilainen, K., Scaubs, P., Zhang, Y. & Liikanen, J.
537 Exploration Targeting and Geological Context of Gold Mineralization in the Neoarchean Ilomantsi
538 Greenstone Belt in Eastern Finland. In: W. D. Maier, R. Lahtinen, & H. O'Brien (Eds). Mineral Deposits of
539 Finland (2015) 435-466. Elsevier Inc.

540 [19] Lehtinen, M. Industrial Minerals and Rocks. In: Maier, W., Lahtinen, R., O'Brien, H. (Eds). Mineral
541 deposits of Finland (2015) 658-705. Elsevier Inc.
542

543 [20] Raith, M.M., Hoffbauer, R., Spiering, R. Shinoto, M., Nakamura, N. Melting behaviour of feldspar clasts
544 in high-fired Sue ware. Eur. J. Mineral. 2016, 28, 385–407 DOI: 10.1127/ejm/2016/0028-2514
545

546 [21] Christidis, G.E. (Ed.), Advances in the characterization of Industrial Minerals. Mineralogical Society of
547 Great Britain and Ireland Vol 9, 2010. https://doi.org/10.1180/EMU-notes.9
548

549 [22] Aasly, K., 2008. Properties and behavior of quartz for the silicon process Thesis for the degree of
550 philosophiae doctor. Norwegian University of Science and Technology. Faculty of Engineering Science and
551 Technology. Department of Geology and Mineral Resources Engineering,
552 https://core.ac.uk/download/pdf/52098782.pdf

553 [23] MacKenzie K.J.D et al. The thermal reactions of muscovite studied by high-resolution solid state 29-Si
554 and 27-Al NMR. Journal of Materials Science 22 (1987) 2645-2654, https://doi.org/10.1007/BF01082158
555
556 [24] Navrotsky, A., Capobianco, C., Stebbins, J. 1982. Some thermodynamic and experimental constraints
557 on the melting of albite at atmospheric and high pressure, J. Geol., 90, 679-698, 1982,
558 https://www.jstor.org/stable/i30081028

559 [25] Johnson, L., McCauley, R. 2005. The thermal behavior of albite as observed by DTA. Thermochimica
560 Acta 437 (2005) 134-139.,

561 [26] Sokolář, R., Vodová, L. Sintering of feldspar rocks from czech quarries. Journal of the Ceramic Society
562 of Japan 123 [1] 62-67 2015

563
564
565
566

567

568